

# Design of a neutron-TPC prototype and its performance evaluation based on an alpha-particle test

HUANG Meng(黄孟)<sup>1</sup> LI Yu-Lan(李玉兰)<sup>1</sup> NIU Li-Bo(牛莉博)<sup>1</sup> LI Jin(李金)<sup>1,2</sup>  
 DENG Zhi(邓智)<sup>1</sup> HE Li(何力)<sup>1</sup> ZHANG Hong-Yan(章洪燕)<sup>1</sup> CHENG Xiao-Lei(程晓磊)<sup>3</sup>  
 FU Jian-Qiang(傅健强)<sup>1</sup> LI Yuan-Jing(李元景)<sup>1</sup>

<sup>1</sup> Dept. of Engineering Physics, Tsinghua University, Key Laboratory of Particle & Radiation Imaging (Tsinghua University), Ministry of Education, Beijing 100084, China

<sup>2</sup> Institute of High Energy Physics, Beijing 100049, China

<sup>3</sup> Nuclear Science and Engineering School, North China Electric Power University, Beijing 102206, China

**Abstract:** A neutron-TPC (nTPC) is being developed for use as a fast neutron spectrometer in the fields of nuclear physics, nuclear reactor operation monitoring, and thermo-nuclear fusion plasma diagnostics. An nTPC prototype based on a GEM-TPC (Time Projection Chamber with Gas Electron Multiplier amplification) has been assembled and tested using argon-hydrocarbon mixture as the working gas. By measuring the energy deposition of the recoil proton in the sensitive volume and the angle of the proton track, the incident neutron energy can be deduced. A Monte Carlo simulation was carried out to analyze the parameters affecting the energy resolution of the nTPC, and gave an optimized resolution under ideal conditions. An alpha particle experiment was performed to verify its feasibility, and to characterize its performance, including energy resolution and spatial resolution. Based on the experimental measurement and analysis, the energy resolution (FWHM) of the nTPC prototype is predicted to be better than 3.2% for 5 MeV incident neutrons, meeting the performance requirement (FWHM<5%) for the nTPC prototype.

**Key words:** fast neutron spectrometer, Monte Carlo simulation, neutron energy resolution

**PACS:** 29.40.Cs, 29.40.Gx, 29.30.Hs **DOI:** 10.1088/1674-1137/39/8/086003

## 1 Introduction

Fast neutron spectrometers with high energy resolution and high detection efficiency are required in some research fields, such as neutron-field characterization, nuclear physics, nuclear reactor operation monitoring, and thermo-nuclear fusion plasma diagnostics [1, 2]. The proton-recoil method is commonly adopted for neutron energy measurement, for its relatively high reaction cross-section compared to other neutron-induced nuclear reactions. Once the recoil proton energy ( $E_p$ ) and the recoil angle ( $\theta$ ) are measured, one can deduce the incident neutron energy by  $E_n = E_p / \cos^2 \theta$ .

Based on the proton-recoil method, several kinds of fast neutron spectrometers have been developed, including proton recoil scintillators, gas proportional counters and proton recoil telescopes [3]. The proton recoil scintillators and gas proportional counters are faced with the complexity of spectrum de-convolution, making it difficult for them to achieve high energy resolutions (commonly FWHM>5%) [3–5]. Through the selection of proton recoil angles in the measurement, proton recoil tele-

scopes can achieve a relatively high resolution (FWHM<5%), but have to pay the price of low detection efficiency ( $\sim 10^{-5}$  or even less) [1, 2, 6].

The neutron-TPC (nTPC) is a fast neutron spectrometer currently being researched, based on a time projection chamber (TPC), with its basic working principle also being the proton-recoil method. As Fig. 1 shows, when the collimated neutron beam enters the effective volume, it has a certain probability of colliding with the nuclei of the hydrogen atoms in the working gas. The recoil proton energy and the recoil angle can be calculated from the energy deposition and the reconstructed track respectively. The incident neutron energy can then be deduced. Compared to conventional neutron spectrometers, the nTPC has the advantages of high n/ $\gamma$  separation ability and a high energy resolution (FWHM<5%) based on current simulations. Meanwhile, its detection efficiency for fast neutrons ( $\sim$ MeV) can reach a medium level ( $\sim 10^{-3}$ ) due to its large effective volume and  $4\pi$  angular coverage [7].

This work will introduce an nTPC prototype being developed at Tsinghua University and present a perfor-

Received 23 October 2014, Revised 10 April 2015

©2015 Chinese Physical Society and the Institute of High Energy Physics of the Chinese Academy of Sciences and the Institute of Modern Physics of the Chinese Academy of Sciences and IOP Publishing Ltd

performance evaluation based on an alpha-particle test. Section 2 presents the design of the nTPC prototype. A Monte Carlo (MC) simulation study based on the Geant4 and Garfield programs is introduced in Section 3 [89]. Section 4 mainly focuses on the performance evaluation of the nTPC prototype. Finally, a conclusion is given in Section 5.

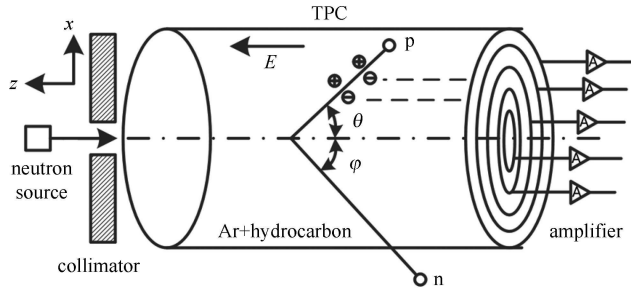


Fig. 1. Schematic diagram of the nTPC.

## 2 Design of the nTPC prototype

The nTPC prototype being developed at Tsinghua University is based on a GEM-TPC (Time Projection Chamber with Gas Electron Multiplier amplification). It has a large cylindrical chamber to allow neutrons to traverse and react inside, with a length of 50 cm and a diameter of 30 cm. In order to ensure the homogeneity of the drift field, a field-cage made of polyimide and copper is installed between the cathode plate and the readout board (see Fig. 2 (left)). A total of 194 copper rings are placed in the inner and outer field-cage, constituting a mirror-ring structure to improve the field uniformity [10]. All the electrodes and the readout detector are placed in a stainless steel barrel whose inner wall has been insulated to avoid sparking with the field-cage. To suppress scattering of the neutrons with the detector material, a rectangular slot was machined on the top of the barrel

as an incident window.

A triple-GEM module is used for electron multiplication, with 1 mm transfer gaps between the GEMs and a 1 mm induction gap between the bottom GEM and the PCB (Printed Circuit Board). The GEMs are made of 50  $\mu\text{m}$  thick kapton foil coated with copper on both sides [11]. The holes on the GEM have a diameter of 50  $\mu\text{m}$  and a spacing of 140  $\mu\text{m}$ . In order to promote the homogeneity of the drift field, especially for the area near the triple-GEM module, a copper guard-ring is placed 7 mm above the top GEM (see Fig. 2 (middle)). The readout board is made of a PCB board, and the pads are ring-distributed with a length ( $\varphi$  direction) of 5 mm and a width ( $r$  direction) of 2 mm (see Fig. 2 (right)). Such a layout is suitable for the measurement of recoil protons, because the projections of proton tracks on the readout board start from the center of the readout pads and extend along the radial direction. In the measurement of 5 MeV neutrons, the drift field should be set as  $\sim 200$  V/cm, and the voltage of each GEM should be around 300 V.

Argon-hydrocarbon mixture is selected as the working gas, serving not only the drift gas of the TPC and the multiplication gas for the GEM, but also the converter for converting neutrons to protons. This design can avoid the energy straggling caused by the introduction of a solid converter, and improve the neutron energy resolution. So far, the plan is to use three kinds of gases in future nTPC running: Ar: $\text{C}_2\text{H}_6$  (50:50), Ar: $\text{CH}_4$  (90:10), and Ar: $\text{CH}_4$  (70:30).

The signals from the pads are read out by an ASIC (Application Specific Integrated Circuit) developed in-house, named CASA-GEM, with a shaping time of 80 ns and a gain of 2 mV/fC. The amplified and shaped signals are sampled with a FADC (Flash Analog-to-Digital Converter, 25 MHz, 12 bits), and transmitted to a computer terminal for further analysis.

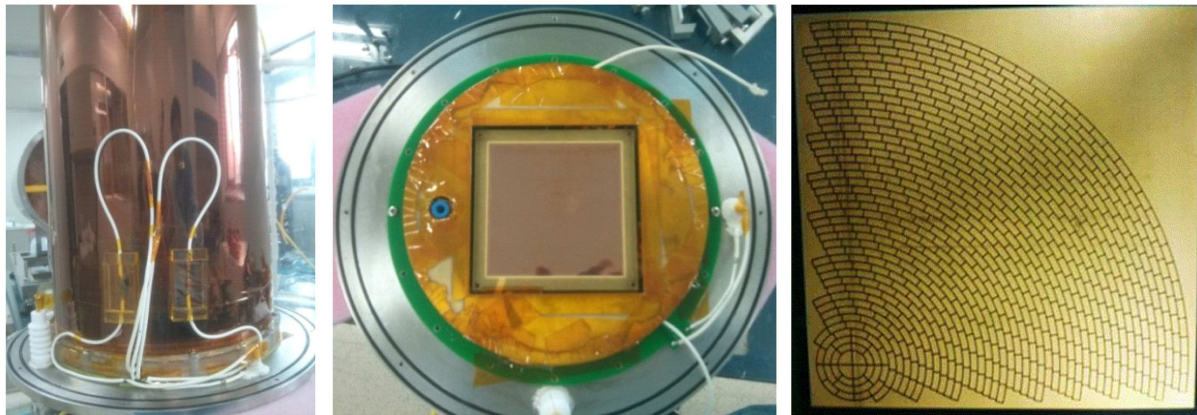


Fig. 2. (color online) Field-cage (left), readout board (middle), and readout pads (right) of nTPC.

### 3 Monte Carlo simulation

A Monte Carlo simulation was carried out to estimate the performance of the nTPC prototype, including energy resolution and detection efficiency. Geant4 was used to simulate the proton recoil and ionization process based on the physics list of QGSP\_BIC\_HP [12], and the energy deposition in the working gas was recorded. The production, drift, and diffusion of secondary electrons, signal generation in pads, retraction of energy and time information were then simulated by Garfield and ROOT programs using the fast MC method [13]. In particular, the time information was given by the time gravity of the signal, and the energy information was given by the number of electrons collected by the readout pad. The track could be reconstructed with the radius of fired pads and the relative drift length of electron clusters. By fitting the proton track, the recoil angle ( $\theta$ ) was deduced. Combined with the energy deposition of the recoil proton in the effective volume, the neutron energy was calculated. The simulation parameters were based on the design of the nTPC prototype introduced in Section 2: the size of the effective volume was  $\phi 300 \text{ mm} \times 500 \text{ mm}$ ; the working gas was Ar:C<sub>2</sub>H<sub>6</sub> (50:50); the drift field was set as 200 V/cm; the readout pads were ring-distributed with 2 mm width; and the energy of the incident neutron beam was 5 MeV.

There are several factors influencing the neutron energy resolution, such as the recoil angle cut ( $\theta_{\text{cut}}$ ) and the fitting track length. First, different recoil angles correspond to different recoil proton energy and different track

lengths. Considering that the neutron energy resolution deteriorates with the decrease of proton energy (or track length), proper selection of the proton events with larger energy deposition (or longer tracks) would improve the neutron energy resolution [7]. As Fig. 3 shows, when the recoil angle cut ( $\theta_{\text{cut}}$ ) becomes larger, the neutron energy resolution deteriorates correspondingly, while the neutron energy efficiency gets better. Note that in Fig. 3 the ratio ( $R$ ) of the number of points ( $N$ ) used in fitting and the whole number of track points ( $N_{\text{all}}$ ) is 0.8.

Second, a smaller fitting track length will reduce the deterioration due to multiple Coulomb scatterings of protons on the accuracy of the reconstructed recoil angle; however, the decrease of the number of fitting points ( $N$ ) will worsen the accuracy of track fitting. Therefore, there should reasonably exist an optimal fitting track length corresponding to the best neutron energy resolution. Based on the simulation results ( $\theta_{\text{cut}}=30^\circ$ ), when the ratio ( $R$ ) of the number of fitting points ( $N$ ) and the whole number of track points ( $N_{\text{all}}$ ) is 0.2, the neutron energy resolution (FWHM) reaches the best ( $\sim 2.2\%$ ) for 5 MeV incident neutrons. Note that the simulation did not take into account electronics noise and the analog-to-digital conversion process; this will be added in future work.

### 4 Alpha-particle test

An alpha particle experiment was set up to verify the basic principles of the proton-recoil method by measuring and reconstructing the energy, the track and the angle of the incident alpha particle. Some characteristics

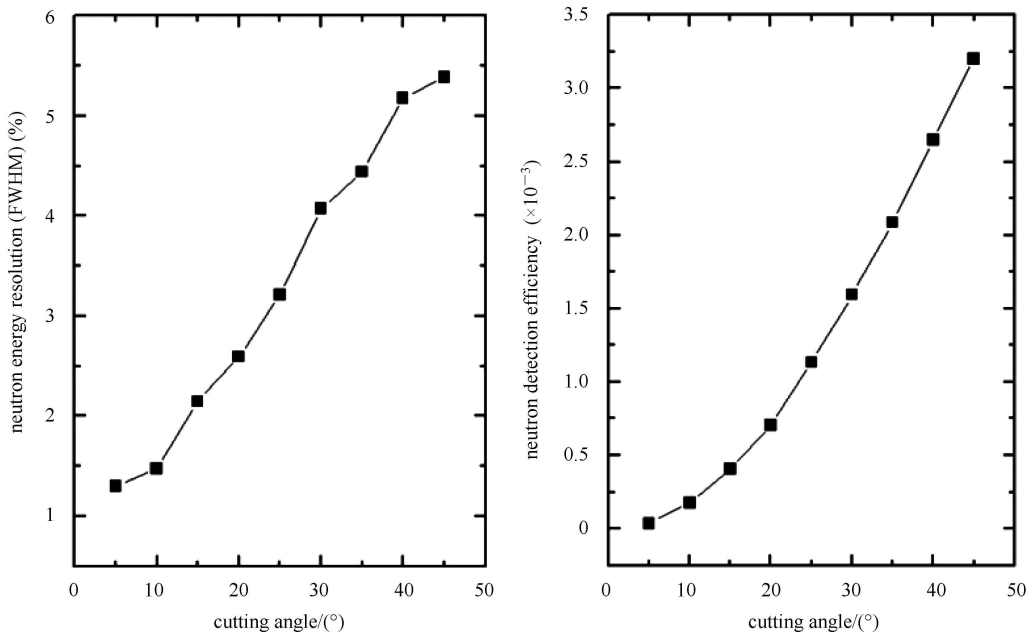


Fig. 3. Neutron energy resolution and detection efficiency vs. cutting angle ( $\theta_{\text{cut}}$ ).

of the nTPC prototype were derived from the experiment data and compared to the simulation results, such as the energy resolution and the spatial resolution. Combined with the analytical method, the neutron energy resolution of the nTPC prototype could be estimated.

#### 4.1 Experimental setup

The schematic of the experimental setup is shown in Fig. 4. An Am-241 alpha source with a radioactivity of  $\sim 10^4$  Bq was placed on top of a collimator made of two stainless steel plates with several circular holes. The holes in the bottom plate were arranged in a line, each hole with a diameter of 0.5 mm. The thickness of the stainless steel plates was 0.2 mm and the gap between the two pieces was 6 mm. The collimator limited the incident angles of alpha particles to several discrete values, that is,  $0^\circ$ ,  $30^\circ$ ,  $45^\circ$  and  $60^\circ$  with the  $z$ -axis. Since the Am-241 alpha source was placed right above the center of the ring-distributed readout pads, the track projections of incident alpha particles on the readout board would extend along the radial direction. Note that all the structures mentioned above were installed inside the effective volume of the nTPC prototype.

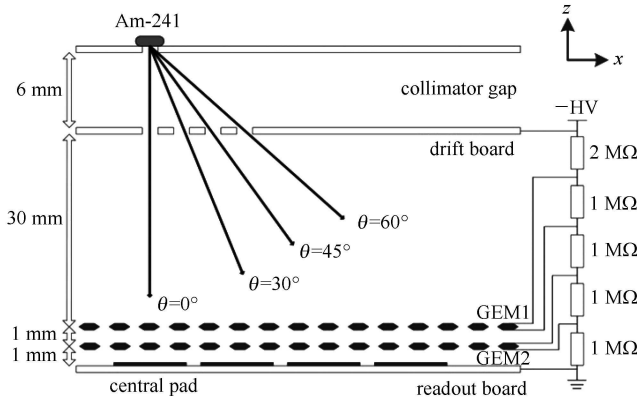


Fig. 4. Schematic of the experiment system.

The working gas of Ar:CH<sub>4</sub> (90:10) was operated in the drift length of 30 mm in the chamber. Considering the higher ionization density of alpha particles than protons, only two GEMs were employed to multiply the secondary electrons. As a result, the cosmic rays and gamma rays from the Am-241 source were hardly detectable, thanks to the relatively low amplification factor of the twin-GEMs. Using a resistor chain, the drift field was set as 186.67 V/cm and the GEM voltage was set as 280 V. The signals from the 48 readout pads were amplified and shaped by the CASA-GEM and fed to the FADC 1724A for analog-digital conversion with a sampling rate of 100 MHz and a quantization resolution of 14 bits. The digitized waveforms were then transmitted to a PC (Personal Computer) terminal for further data processing.

In the experiment, the nTPC prototype worked in event-by-event mode triggered by the cathode signal, which was read out from the bottom side of the lower GEM and fed into a threshold discriminator. The data acquisition lasted about 4 hours, and the room temperature was kept approximately constant by an air conditioner.

#### 4.2 Experiment results and analysis

##### 4.2.1 Calibration of the DAQ system and preprocessing of the raw data

As the first step, the gains of the 48 electronics channels were calibrated by measuring the response functions of the output amplitudes (or integration area) with the input charges. Since the lengths of the cables for triggering the six FADC 1724A boards were different, the resulting inconsistency of triggering latency also needed correction. By injecting triggering signals into six FADC 1724A boards from a common signal generator and comparing the timing deviations, the inconsistency of triggering latency among the different FADC boards was adjusted.

After the calibration of the DAQ (Data Acquisition System) system, the raw waveforms recorded were pre-processed, including saturation cut, baseline subtraction, threshold setting, and preliminary selection of true signals. In particular, in order to exclude signals induced by environmental interference, a requirement of signals with pulse-widths wider than 500 ns was set. Having been verified by the following data processing, nearly all signals meeting the pulse-width requirement were from real alpha particle events. Then, the energy information was extracted by summing the integration area of the waveform above the threshold, and the time information was deduced based on the constant fraction timing method. Both energy and time information were stored in a ROOT file for further processing.

##### 4.2.2 Energy resolution of alpha particles

The Am-241 alpha particle source used in the experiment had gold plating on the surface, resulting in different energy losses of alpha particles passing through it [14]. In order to find out the influence of the plating on the particle energy, a Si surface barrier detector was employed to measure the energy spectrum of outgoing alpha particles. The spectrum was found to be approximately Gaussian with an energy of  $4.516 \text{ MeV} \pm 0.227 \text{ MeV}$  ( $\text{FWHM} \approx 11.8\%$ ). Based on the measurement results, the thickness of the gold plating was derived as  $\sim 2 \mu\text{m}$ , agreeing well with the data in Ref. [14].

Figure 5 shows the energy spectra of alpha particles measured in the experiment, where the integration areas of signal waveforms are used to represent the energy information of signals. For alpha particles with an incident angle of  $30^\circ$ , the energy resolution (FWHM) was

14.0% (see Fig. 5(a)), while it was 19.1% for particles at an incident angle of  $45^\circ$  (see Fig. 5(b)). The energy straggling measured was mainly caused by 4 factors: the intrinsic energy straggling of the alpha particles from the source caused by the gold plating as the dominant factor; the straggling of energy loss in the collimator gap; the statistical fluctuation of the number of electrons in the ionization and avalanche processes; and electronics noise.

### 4.2.3 Reconstruction of alpha particle tracks

Based on the energy and time information of the signals, the alpha particle tracks in the drift chamber could be reconstructed. A signal from a pad with amplitude higher than the threshold was regarded as a hit. Fig. 6(a) shows the hits of an alpha particle using a grayscale image: the darker the color of the pads, the

more electrons collected. Hits on the same arc were combined as a cluster, with the cluster's position on the  $r$ -direction the same as the hits, and its position on the arc-direction determined by the charge gravity of the hits. Besides, the  $z$ -coordinate of the cluster was the product of the time gravity of hits and the drift velocity of electrons ( $5.2389 \text{ cm}/\mu\text{s}$ , calculated by the Garfield program). Fig. 6(b) shows the energy depositions of an alpha particle along the  $r$ -direction, responding to the energy of clusters. In the figure the Bragg peak can be seen clearly. Since the alpha particle's track has a certain tilt angle with the readout board, the tail of the Bragg peak in Fig. 6(b) is not as steep as that of the energy deposition along the track. Besides, the pad width of 2 mm also contributes to the slow decline of the tail of the Bragg peak measured.

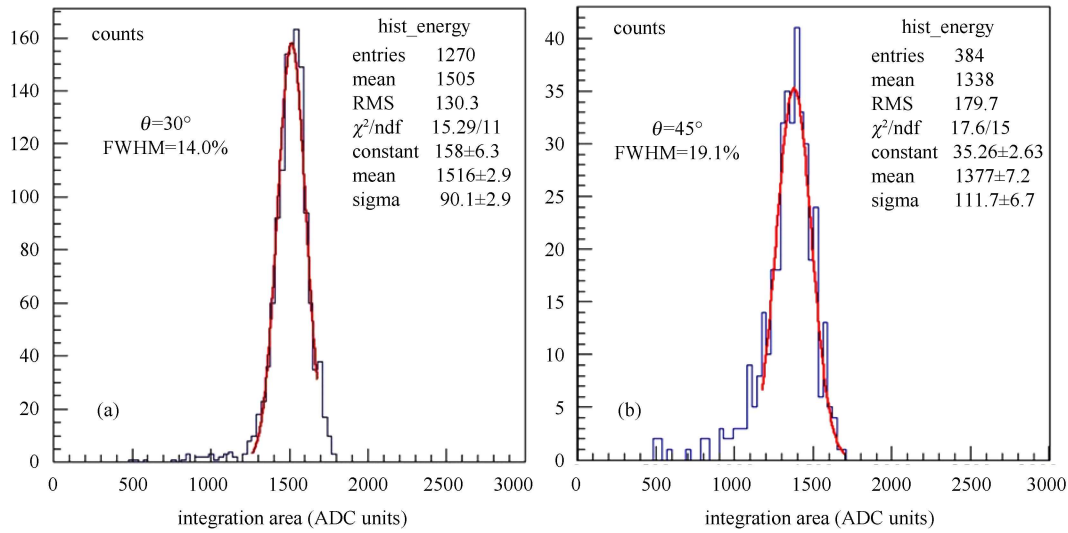


Fig. 5. (color online) Measured energy spectra of alpha particles with incident angles of  $30^\circ$  (a) and  $45^\circ$  (b).

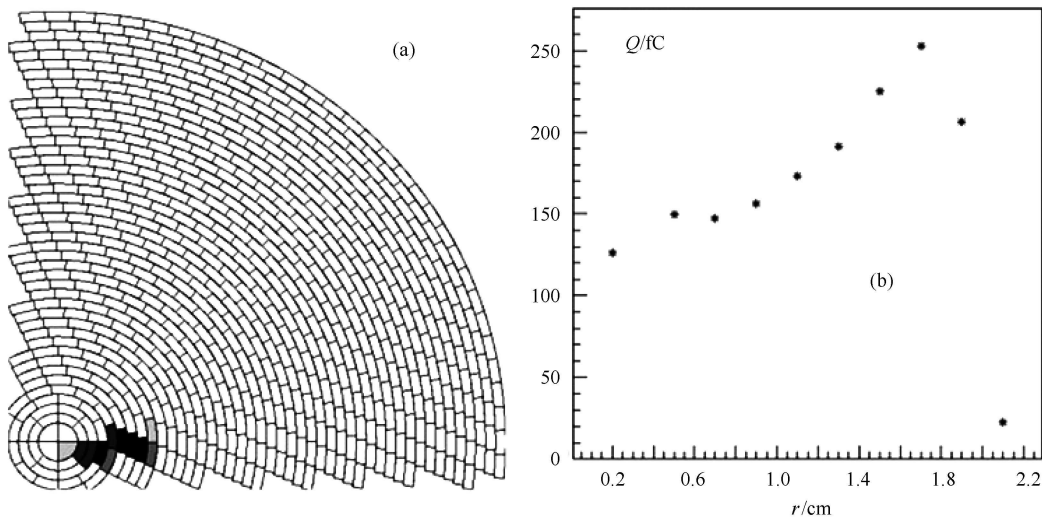


Fig. 6. Hits (a) and energy depositions (b) of an alpha particle.

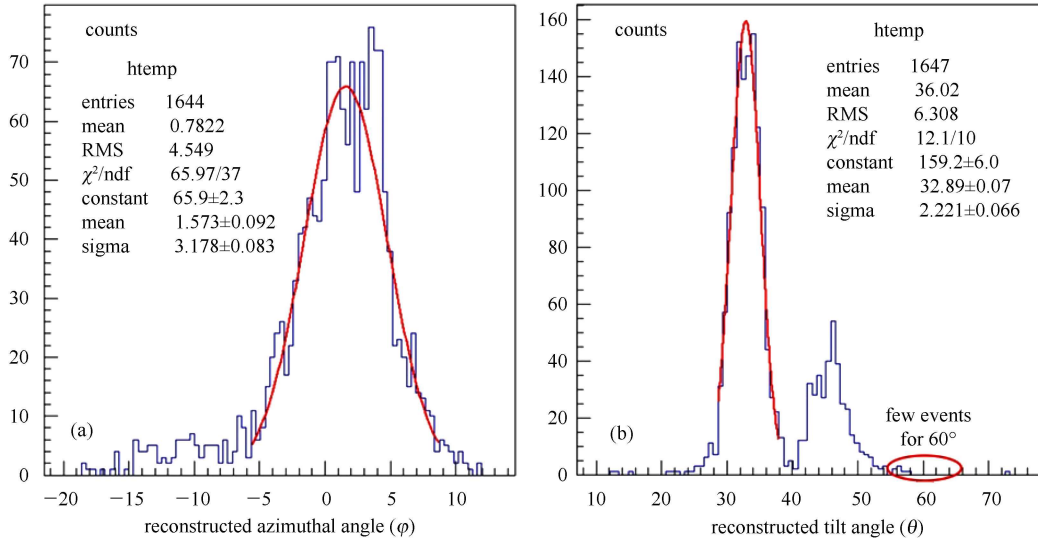


Fig. 7. (color online) Distributions of the reconstructed azimuthal angles ( $\varphi$ ) and tilt angles ( $\theta$ ).

By fitting the positions of clusters on the  $x$ - $y$  plane using a linear function, the angle of the projected alpha particle's track with the  $x$ -axis could be reconstructed, defined as the azimuthal angle ( $\varphi$ ). Fig. 7(a) shows the distribution of the reconstructed azimuthal angles ( $\varphi$ ), with a central value of  $1.573^\circ \pm 0.092^\circ$  and resolution (standard deviation) of  $3.178^\circ \pm 0.083^\circ$ . Then, the tilt angles of alpha particles ( $\theta$ ) with the  $z$ -axis could be derived by fitting the cluster positions on the  $r$ - $z$  plane using a linear function, whose slope was equivalent to  $\tan \theta$ . As Fig. 7(b) shows, the central values (standard deviations) of the reconstructed tilt angles are  $32.89^\circ \pm 0.07^\circ$  ( $2.221^\circ \pm 0.066^\circ$ ) and  $45.72^\circ \pm 0.15^\circ$  ( $2.468^\circ \pm 0.123^\circ$ ), corresponding to the collimator angles of  $30^\circ$  and  $45^\circ$  respectively. Note that for the collimator angle of  $60^\circ$ , the alpha particle events detected were rare, since the actual collimator channels became narrower with the collimator angle increasing, resulting in fewer alpha particles outgoing from the collimator.

Table 1. Central values of angle distributions of alpha particles from simulation and experiment.

	simulation	experiment
azimuthal angle ( $\varphi$ )	$0^\circ$	$1.573^\circ \pm 0.092^\circ$
tilt angle ( $\theta$ )	$29.48^\circ \pm 0.07^\circ$	$32.89^\circ \pm 0.07^\circ$
	$44.47^\circ \pm 0.06^\circ$	$45.72^\circ \pm 0.15^\circ$

In order to evaluate the accuracy of the reconstructed angles, a simulation based on the Geant4 program was carried out to calculate the distributions of tilt angles and azimuthal angles of alpha particles outgoing from the collimator. The geometry in the simulation was based on the real design of the collimator, and the incident alpha

particles ( $10^6$  particles) were isotropic. The central values of outgoing angle distributions were calculated and compared to the reconstruction results as shown in Table 1. It is obvious that the reconstruction results are very close to the simulation results, proving the correctness and accuracy of the experiment.

#### 4.2.4 Evaluation of energy resolution of the nTPC prototype

The  $z$ -resolution of the nTPC was calculated based on the linear fitting of alpha particle tracks on the  $r$ - $z$  plane. The difference between the reconstructed cluster position on the  $z$ -axis and the corresponding value of the fitting function was defined as the  $z$ -residual, and its standard deviation was equivalent to the  $z$ -resolution. As Fig. 8 shows, the  $z$ -resolution of the nTPC in the drift chamber ( $0 \leq z \leq 3$  cm) is  $271.2 \mu\text{m} \pm 2.7 \mu\text{m}$  and  $370.1 \mu\text{m} \pm 4.3 \mu\text{m}$  for alpha particles with tilt angles of  $30^\circ$  and  $45^\circ$  respectively. The  $z$ -resolutions are mainly affected by the inhomogeneity of the drift field, electronics noise, and the track angle effect [15]. Based on the  $z$ -resolution measured, the neutron energy resolution of the nTPC prototype can be evaluated with analytical methods, with the detailed derivation process as follows.

Firstly, the neutron energy resolution of the nTPC is determined by three factors: the proton energy resolution  $\left(\frac{\sigma_{E_p}}{E_p}\right)$ , the standard deviation of the slopes ( $k$ ) of proton tracks caused by multiple Coulomb scattering ( $\sigma_{k(\text{scat})}$ ), and by the track fitting accuracy ( $\sigma_{k(\text{fit})}$ ). The term  $\left(\frac{\sigma_{E_p}}{E_p}\right)$  can be estimated based on the number of electrons collected by the readout pads, as the following

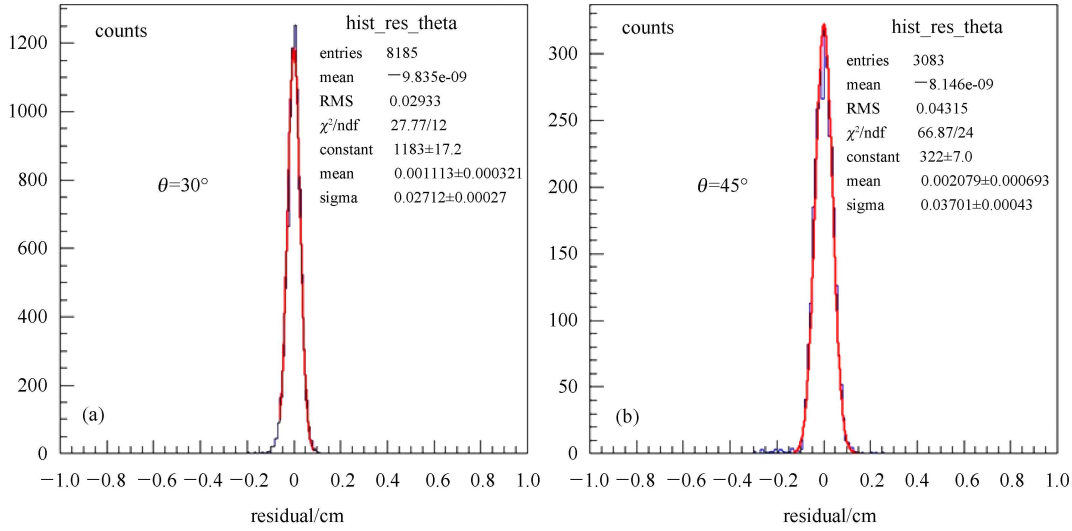


Fig. 8. (color online) Distributions of residuals on the  $r$ - $z$  plane.

equation shows:

$$\left(\frac{\sigma_{E_n}}{E_n}\right)^2 = \frac{\bar{W}}{E_n} \left(1 + \frac{1}{k^2}\right) \left(F + \frac{\sigma_A^2}{\langle A \rangle^2}\right) + \left(\frac{-2\sigma_{k(\text{scat})}}{k^3+k}\right)^2 + \left(\frac{-2\sigma_{k(\text{fit})}}{k^3+k}\right)^2, \quad (1)$$

where  $k = \tan(\theta + \pi/2) = -1/\tan\theta$ ,  $F$  is the Fano factor,  $\bar{W}$  is the average ionization energy, and  $\frac{\sigma_A^2}{\langle A \rangle^2}$  is the relative variance of the amplification factor ( $A$ ) of the triple GEM module.

Secondly, the term  $\sigma_{k(\text{scat})}$  can be estimated using the Highland formula [16]:

$$\sigma_\varphi = \frac{13.6 \text{ MeV}}{\beta pc} z \sqrt{\frac{l_0}{X_0}} \left[1 + 0.038 \ln\left(\frac{l_0}{X_0}\right)\right], \quad (2)$$

$$\sigma_{k(\text{scat})} = \frac{\sigma_\varphi}{\sqrt{3}} (1+k^2), \quad (3)$$

where  $\varphi$  is defined as the angle between the initial direction of the recoil proton and its final direction after passing through a material with a certain thickness,  $l_0$  is the areal density of the material,  $X_0$  is the radiation length of the material,  $\beta$  is the velocity of the recoil proton,  $p$  is the momentum of the proton,  $z$  is the atomic number of the proton, and  $c$  is the speed of light.

Lastly, the term  $\sigma_{k(\text{fit})}$  can be calculated based on the following equation [17]:

$$\sigma_{k(\text{fit})}^2 = \frac{\sum_{i=1}^N \frac{1}{\sigma_{z_i}^2}}{\sum_{i=1}^N \frac{1}{\sigma_{z_i}^2} \cdot \sum_{i=1}^N \frac{r_i^2}{\sigma_{z_i}^2} - \sum_{i=1}^N \frac{r_i}{\sigma_{z_i}^2} \cdot \sum_{i=1}^N \frac{r_i}{\sigma_{z_i}^2}}, \quad (4)$$

where  $N$  is the number of fitting points,  $r_i$  and  $z_i$  are the  $r$ -coordinate and  $z$ -coordinate of the fitting track point

respectively, and the  $\sigma_{z_i}$  is the  $z$ -resolution of nTPC at  $z = z_i$ . In detail, the  $z$ -resolution of nTPC can be given by:

$$\sigma_z^2 = \sigma_{\text{det}}^2 + \sigma_{\text{ele}}^2 + \frac{d^2}{12 \cdot \tan^2 \theta \cdot N_{\text{eff}}} + \frac{D_L^2}{N_{\text{eff}}} z, \quad (5)$$

where  $\sigma_{\text{det}}$  represents the intrinsic detector resolution related to the readout pads layout, the uniformity of drift electric field, the GEM module setting, and so on;  $\sigma_{\text{ele}}$  includes the influences of the analog-digital converting process and electronics noise; the third term is influenced by the tilt angle of the proton track with  $z$ -axis [15], where  $d$  is the pad width,  $\theta$  is the tilt angle of the proton track (also the proton scattering angle), and  $N_{\text{eff}}$  is the effective electron number; the fourth term is caused by the longitudinal diffusion of electrons [18], where  $D_L$  is the longitudinal diffusion coefficient of the working gas, and  $z$  is the distance from the original position of ionized electrons to the readout board.  $N_{\text{eff}}$  can be given by the following formula [18]:

$$N_{\text{eff}} = \frac{1}{\langle A^2 \rangle \cdot \langle \frac{1}{N} \rangle} = \frac{1}{\left(1 + \frac{\sigma_A^2}{\langle A \rangle^2}\right) \cdot \langle \frac{1}{N} \rangle} = \frac{1}{\langle \frac{1}{N} \rangle} \left(\frac{1+\alpha}{2+\alpha}\right), \quad (6)$$

where  $A$  is the amplification factor of the GEM module,  $N$  is the number of drift electrons per pad row, and  $\alpha$  is the parameter determining the shape of the Polya distribution that the amplification factor ( $A$ ) obeys. Note that some deviation in the estimation of the energy resolution of the nTPC prototype might be brought in, since the estimation of  $N_{\text{eff}}$  is not accurate enough to make a distinction between twin-GEMs and triple-GEMs.

From the experimental results, the term  $\sigma_{\text{det}}^2 + \sigma_{\text{ele}}^2$  equals about  $(300 \mu\text{m})^2$  for the nTPC prototype with twin-GEMs. Since the difference between the influence of twin-GEMs and triple-GEMs on the energy resolution of nTPC is relatively small compared to other influencing factors, such as the electron diffusion in the drift area, the term  $\sigma_{\text{det}}^2 + \sigma_{\text{ele}}^2$  for the nTPC prototype with triple-GEMs is also approximately equal to  $(300 \mu\text{m})^2$ .

Based on the equations above, when the recoil angle cut is  $30^\circ$  and the ratio ( $R$ ) is 0.2, then it is possible to obtain a neutron energy resolution (FWHM) of 3.2% for the nTPC prototype with 5 MeV incident neutrons, meeting the performance requirement (FWHM<5%) for the nTPC prototype. Compared to the simulation results (FWHM $\approx$ 2.2%), the neutron energy resolution derived based on the experimental results is worse, since the simulation does not take into account all possible factors, including the inhomogeneity of the drift field and GEM

multiplication, the machining accuracy of the detector, and electronics noise.

## 5 Conclusion

An nTPC prototype based on a GEM-TPC is being developed at Tsinghua University. A triple-GEM module is employed to avalanche the electrons ionized by recoil protons in a working gas of argon-hydrocarbon mixture. Based on fast MC simulation, the energy resolution (FWHM) of the nTPC for 5 MeV neutrons was estimated as  $\sim$ 2.2%. An alpha particle experiment was carried out to verify its feasibility, and to characterize its performance. Based on the experimental data and further analysis, it is possible to reach an energy resolution (FWHM) of 3.2% for the nTPC prototype with 5 MeV incident neutrons, meeting the performance requirement (FWHM<5%) for the nTPC prototype.

## References

- 1 Matsumoto T et al. IEEE Nuclear Science Symposium Conference Record, 2004, **2**: 715–719
- 2 Chizuo M et al. Nucl. Instrum. Methods A, 1999, **422**: 75–78
- 3 Knoll G F. Radiation Detection and Measurement. Third edition. New York: John Wiley & Sons Inc., 1999. 537–576
- 4 Singkarat S, Garis N S, Grosshög G. Nucl. Instrum. Methods A, 1993, **335**: 248–254
- 5 Pichenot G et al. Nucl. Instrum. Methods A, 2002, **476**: 165–169
- 6 Hawkes H P et al. Nucl. Instrum. Methods A, 2002, **476**: 506–510
- 7 HUANG Meng et al. IEEE Nuclear Science Symposium and Medical Imaging Conference (NSS/MIC), 2012. 146–148
- 8 Agostinelli S et al. Nucl. Instrum. Methods A, 2003, **506**: 250–303
- 9 Veenhof R. Nucl. Nucl. Instrum. Methods A, 1998, **419**: 726–730
- 10 ZHENG Bao-Jun et al. Chinese Physics C, 2011, **35**(1): 56–60
- 11 Sauli F. Nucl. Nucl. Instrum. Methods A, 1997, **386**: 531–534
- 12 [http://geant4.cern.ch/support/proc\\_mod\\_catalog/physics\\_lists/referencePL.shtml](http://geant4.cern.ch/support/proc_mod_catalog/physics_lists/referencePL.shtml)
- 13 ROOT. A Data Analysis Framework. <http://root.cern.ch/>
- 14 FENG Gen-Sheng, WANG Ying, FENG Xin-Zhan. Journal of Isotopes, 1998, **11**(2): 22–26 (in Chinese)
- 15 Kobayashi M et al. Nucl. Instrum. Methods A, 2011, **641**: 37–47
- 16 Bichsel H, Groom D E, Klein S R. The European Physical Journal C - Particles and Fields, 2000, **15**(1–4): 163–173
- 17 LI Yao-Qing. Experimental Data Processing. Hefei: Press of USCT, 2003. 130–139 (in Chinese)
- 18 LI Yu-Lan. The Design, Construction and Experimental Study of a GEM-TPC Prototype, (Ph. D. Thesis). Beijing: Tsinghua University, 2007 (in Chinese)